2007-01-2179

Errors Associated with Transfer Path Analysis when Rotations are not Measured

Akira Inoue and Rajendra Singh
Acoustics and Dynamics Laboratory, The Ohio State University

ABSTRACT

Previously we had found significant errors in the interfacial force results for a source-path-receiver system where only translational motions were measured. This paper examines the sources of those errors by using computational finite and boundary element models. The example case consists of a source structure (with few modes), a receiver (with many modes) and three steel rod paths. We first formulate indirect, yet exact, methods for estimating interfacial forces, by assuming that six-dimensional motions at any location are available though we focus on only the driving points. One- and three-dimensional sub-sets of the proposed formulation are compared with the six-dimensional theory in terms of interfacial force and partial sound pressure spectra.

INTRODUCTION

The structure-borne noise transfer path analysis (TPA) method utilizes interfacial path forces $F_i(\omega)$ at frequency ω (rad/s) to determine partial sound pressures $p_i(\omega)$ as: $p(\omega) = \sum_i p_i(\omega) = \sum_i \left(\partial p / \partial F_i\right) F_i$, where $p(\omega)$ is the (total) sound pressure at a receiver location, $\partial p / \partial F_i$ is acoustic frequency response function, and *i* is the path (and direction) index [1-4]. However, it is often difficult to directly measure in-situ path forces in real-life systems, and thus an indirect estimation method must be implemented [5-7]. Recently we demonstrated a TPA experiment using a 2-chamber system [2], where directly measured path forces were compared with indirect estimations. However, significant errors were found in many frequency bands.

For linear systems, the expansion $F_i(\omega) = \sum_n \left(\partial F_i / \partial a_n\right) a_n$ should converge to the interfacial force of the *i*th path when *n* is sufficiently high, provided all necessary motions (given by dimension *d* at any location) have been measured. Here, $a_n(\omega)$ is the dynamic acceleration, and *n* is the (path) location and direction index. In general, one should consider *d* = 6 at each point [8]. However, the real-life structural measurements are usually limited to the translational directions only (*d* = 3), though many are made only in the vertical direction (*d* = 1), due to the technical difficulties associated with rotational measurements [9,10]. Therefore, the following fundamental question arises: Can we truly quantify the structure-borne noise paths in a system without considering rotational motions? We will address this particular issue via an example case.

PROBLEM FORMULATION

Specific objectives of this paper are as follows. 1. Develop a simplified multi-path structure with mismatched modes between the source and the receiver regimes, which can be typically found in many real-life systems. 2. Establish indirect, yet exact, interfacial path force estimation methods formulated by using only the driving point responses and FRFs. 3. Estimate the effects of the ignored dimensions, especially the rotational motions, on path force, partial sound pressure, and power flow spectra. The scope of this paper is limited to a linear time-invariant (LTI) discretized system, and only the steady-state harmonic responses will be studied in the frequency domain. The ubiquitous $e^{j\omega t}$ terms are omitted for the sake of brevity.

In the indirect force estimation method, the measured structural compliance type frequency response function (FRF) matrix is computationally inverted at each frequency, and hence it is referred to as the matrix inversion method [6]. Several researchers have tried to refine this method. However, a common drawback is that only the translational motions are typically utilized in the experimental TPA studies [2,3]. Since the exact formulation has been never used, the effect of the missing dimensions is unknown though it could be considerable. Consequently, the estimation scheme and subsequent analyses are often costly trial and error approaches. In order to quantify and hopefully reduce the estimation errors, we propose indirect, yet exact, interfacial force estimation methods that include 6-dimensional motions (3 translations and 3 rotations) at any location. Then we estimate the errors committed by limited dimensional formulations.

EXAMPLE CASE

We have developed a simplified structure with multiple parallel paths, as shown in Figure 1. In typical vibration isolation problems, the source structure has only few modes over the frequency range of interest. For instance, an automotive engine could be modeled purely as a rigid body element at low frequency range. On the other hand, the receiver structure (like a compliant chassis) has so many modes over the same frequency range. Such a mismatch in terms of the mode counts can be seen in many practical systems. The source and receiver regimes are usually connected by multiple mounts or structural connections [11].

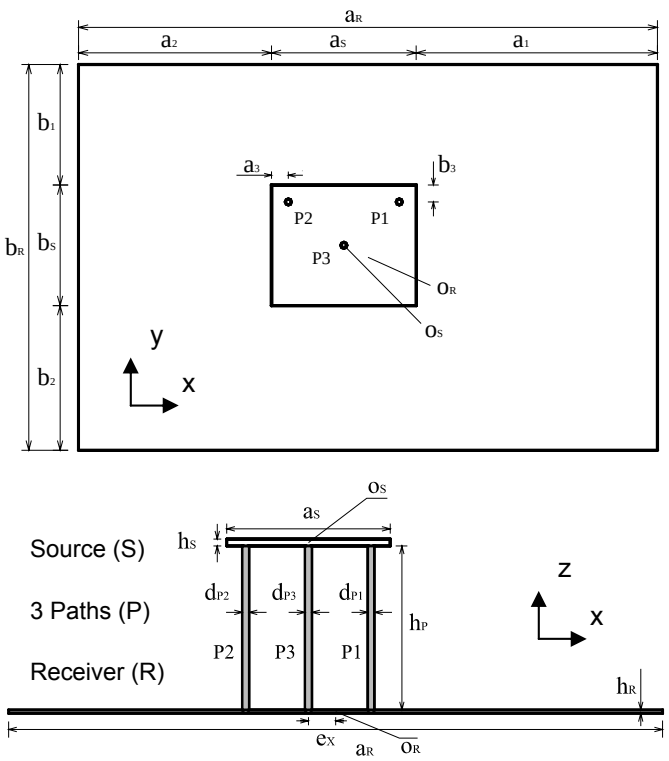

Figure 1. Example case with three parallel paths. Dimensions (all in mm) are as follows: a_S = 152.4, a_R = 609.6, a_1 = 254.0, a_2 = 203.2, a_3 = 17.8, b_S = 127.0, b_R = 406.4, b_1 = 127.0, b_2 = 152.4, b_3 = 17.8, d_{P1} = d_{P2} = d_{P3} = 6.350, e_X = 25.4, e_Y = 12.7, h_S = 6.350, h_P = 152.4, h_R = 3.175. Key: O_S, center of mass of the source plate; O_R, center of mass of the receiver plate.

The source (S) structure of Figure 1 is a thick steel plate, which has very few modes up to 3 kHz, though the effects of shear deformation and rotary inertia are considered. In contrast, the receiver (R) structure is a thin compliant steel plate, which has many modes. In order to observe effects of rotational motions, three path (P) beams are installed in a triangular configuration, as is seen in Figure 1, which we designate as the 3-path system. Each path is a circular rod (152.4 mm long and 6.350 mm diameter) made of steel. An impulsive force is applied in the vertical z-direction (parallel to the paths) at the lower right corner of the source plate. The force amplitude at any frequency may be treated as F = (0,0,1) (N) over the applicable range of interest.

We have conducted modal and frequency response tests to validate the computational models. For instance, Figure 2 compares accelerance spectra on a narrow band basis obtained by finite element model and experiment. Although some natural frequency shifts are observed (especially at the lower frequencies), good agreement is found between model and experiment. Thus, we will utilize the computational model for subsequent analyses.

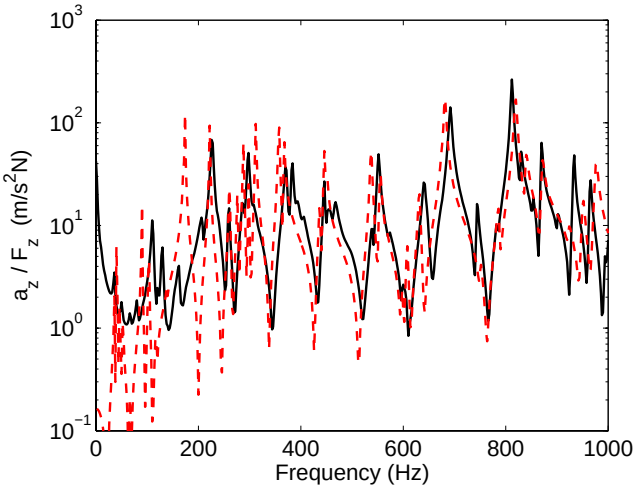

Figure 2. Driving point accelerance of the example case of Figure 1 on narrow band basis. Key: ———, experiment; — — —, model.

We analyze this example by using the finite element method (FEM) and the boundary element method (BEM) [12,13], discretizing both plates and rods. We start from the indirect, yet exact, formulation with 6 degree-of-freedom (DOF), 3 translational and 3 rotational motions, at each point (node) to estimate interfacial forces through 3 paths. This is designated as the 6DOF formulation. Then, we analyze the experimental paradigm, where only the vertical motions are measured, which corresponds to the 1DOF formulation. Furthermore, two intermediate 3DOF formulations are also investigated. The 1 and 3DOF formulations are compared with the exact 6DOF formulation in terms of accuracy.

The governing equations of motion, in matrix form in frequency domain, may be generally written as $\mathbf{D}(\omega)\mathbf{Q}(\omega)=\mathbf{F}(\omega)$. Here, $\mathbf{Q}(\omega)=\{\mathrm{X},\mathrm{Y},\mathrm{Z},\Psi,\Theta,\Phi\}^{\mathrm{T}}$ is the complex displacement amplitude vector of dimension 6 at any location; Ψ, Θ and Φ correspond to the complex angular displacements (in rad) about x, y and z axes, respectively. $\mathbf{F}(\omega)$ = (F_x, F_y, F_z, N_ψ, N_θ, N_ϕ) is the complex external harmonic force (F) and moment (N) amplitude vector. $\mathbf{D}(\omega)$ $\left(=\left[F/Q\right]\right)$ is the dynamic stiffness matrix. The response is given by $\mathbf{Q}=\mathbf{D}^{-1}\mathbf{F}=\mathbf{H}\mathbf{F}$, where $\mathbf{H}(\omega)$ $\left(=\left[Q/F\right]\right)$ is the compliance matrix ($\mathbf{H}(\omega)=\mathbf{D}^{-1}(\omega)$). The bold symbol indicates a matrix or vector.

INDIRECT FORCE AND PARTIAL PRESSURE ESTIMATION METHODS

First, dynamic force and moment between two adjacent structural points, say *m* and *n,* is given as:

$$\mathbf{F}_{mn} = -\tilde{\mathbf{k}}(\mathbf{Q}_m - \mathbf{Q}_n) \qquad (1)$$

where $\tilde{\mathbf{k}}$ $(=\mathbf{k} + j\omega\mathbf{c})$ is complex stiffness matrix between the 2 points (off-diagonal terms are ignored). Path force estimation given by Equation (1) may be called as the direct method. However, when the stiffness of a path is very high, the result could contain significant error due to very small difference between the displacements $(\mathbf{Q}_m \approx \mathbf{Q}_n)$ [1]. Also, one must have the knowledge of "in-situ" $\tilde{\mathbf{k}}$ values for practical applications. However, it is a difficulty to carry out the direct method and thus an indirect method must be employed.

In order to indirectly yet exactly estimate the interfacial path forces $\mathbf{F}_i$ (*i* = 1, 2, 3) at the source-path (S-P) junctions of the system of Figure 1, the equations of motion for the all discretized points (nodes) of the path-receiver (P-R) sub-system are considered as $\mathbf{D}_{\text{P-R}}\mathbf{Q} = \mathbf{F}$, where the interfacial path forces from the source structure are regarded as external forces. Note that the FRF matrix $\mathbf{D}_{\text{P-R}}$ has to be evaluated without the source structure as indicated by the subscript P-R, and $\mathbf{F}$ and $\mathbf{Q}$ are the force and response evaluated in the entire S-P-R system under the operational condition. Also, note that $\mathbf{D} \neq \mathbf{H}^{-1}$ in general, and $D_{m,n} \neq H_{n,m}^{-1}$ for each component, where $D_{m,n} = F_m / Q_n$ and $H_{n,m} = Q_n / F_m$, because of the difference in the boundary conditions. However, $\mathbf{D}_{\text{P-R}} = \mathbf{H}_{\text{P-R}}^{-1}$ holds, because $\mathbf{D}_{\text{P-R}}$ and $\mathbf{H}_{\text{P-R}}$ completely determine the dynamics of the all points of the P-R sub-system. If FRFs and responses of the all discretized points of the P-R sub-system in this equation were known, the interfacial path forces at the S-P junctions would be exactly estimated, though it is not realistic for actual systems. Thus, we re-arrange the equations of motion for the P-R sub-system only about the S-P junctions (designated as the driving points) as follows. [14]

$$\begin{pmatrix}\mathbf{F}_1\\ \mathbf{F}_2\\ \mathbf{F}_3\end{pmatrix} = \begin{pmatrix}\mathbf{H}_{1,1} & \mathbf{H}_{1,2} & \mathbf{H}_{1,3}\\ \mathbf{H}_{2,1} & \mathbf{H}_{2,2} & \mathbf{H}_{2,3}\\ \mathbf{H}_{3,1} & \mathbf{H}_{3,2} & \mathbf{H}_{3,3}\end{pmatrix}_{\text{P-R}}^{-1} \begin{pmatrix}\mathbf{Q}_1\\ \mathbf{Q}_2\\ \mathbf{Q}_3\end{pmatrix} \qquad (2)$$

$$= \begin{pmatrix}\mathbf{D}_{1,1} & \mathbf{D}_{1,2} & \mathbf{D}_{1,3}\\ \mathbf{D}_{2,1} & \mathbf{D}_{2,2} & \mathbf{D}_{2,3}\\ \mathbf{D}_{3,1} & \mathbf{D}_{3,2} & \mathbf{D}_{3,3}\end{pmatrix}_{\text{P-R}} \begin{pmatrix}\mathbf{Q}_1\\ \mathbf{Q}_2\\ \mathbf{Q}_3\end{pmatrix} \qquad (3)$$

All F, Q, H and D terms of Equations (2) and (3) are evaluated at the driving points only. The above set of equations also completely determines the dynamics of the all driving points, and thus $\mathbf{D}_{\text{P-R}}\big|_{\text{Dr}} = \mathbf{H}_{\text{P-R}}\big|_{\text{Dr}}^{-1}$ holds, where subscript Dr indicates the driving points. Because there are 3 paths and 6 dimensional motions are counted, 18 by 18 matrices are found. Equation (2) also gives an indirect exact interfacial force formulation at the S-P junctions (designated as the indirect method) using only the driving point FRFs and responses. Figure 3 shows interfacial force (in the z-direction) spectra of path 3 on narrow band basis as estimated by two alternative formulations (1) and (2). Results show that direct and indirect methods yield the same spectra with an average error of 0.01% for the path force. Thus, it may be concluded that the indirect method (6DOF formulation based on Equation (2)) exactly estimate the interfacial path forces and moments.

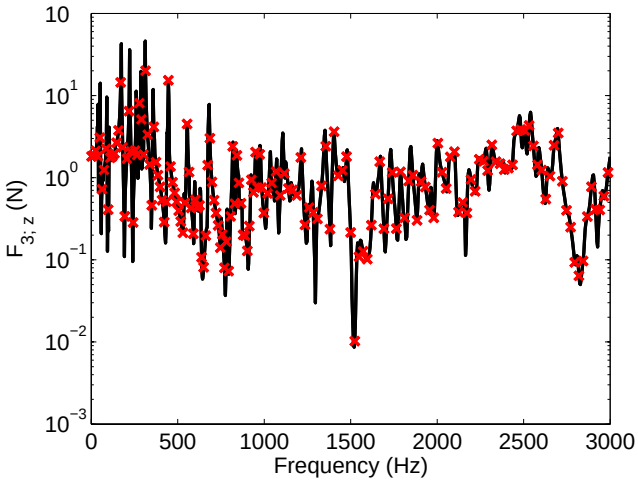

Figure 3. Interfacial force magnitude spectra in the z-direction at the junction of source and path 3 (on narrow band basis). Key: ——, direct method by Equation (1); **X**, indirect method by Equation (2).

After the matrix inversion in Equation (2), the force/moment of path *i* in *q*-dimension (*q* = *x, y, z, ψ, θ, φ*) in Equation (3) may be expanded as

$$\begin{aligned}\mathrm{F}_{i;\,q} &= \sum_{Q=X,Y,Z,\Psi,\Theta,\Phi}\ \sum_{n=1}^{3} \mathrm{F}_{i;\,q;\,Q_n}\\ &= \sum_{n=1}^{3}\left(\frac{\mathrm{F}_{i;\,q}}{X_n}\bigg|_{\substack{\bar{Q}=0\\ \text{except } X_n}} X_n + \frac{\mathrm{F}_{i;\,q}}{Y_n}\bigg|_{\substack{\bar{Q}=0\\ \text{except } Y_n}} Y_n \right.\\ &\quad + \frac{\mathrm{F}_{i;\,q}}{Z_n}\bigg|_{\substack{\bar{Q}=0\\ \text{except } Z_n}} Z_n + \frac{\mathrm{F}_{i;\,q}}{\Psi_n}\bigg|_{\substack{\bar{Q}=0\\ \text{except } \Psi_n}} \Psi_n \qquad (4)\\ &\quad \left. + \frac{\mathrm{F}_{i;\,q}}{\Theta_n}\bigg|_{\substack{\bar{Q}=0\\ \text{except } \Theta_n}} \Theta_n + \frac{\mathrm{F}_{i;\,q}}{\Phi_n}\bigg|_{\substack{\bar{Q}=0\\ \text{except } \Phi_n}} \Phi_n \right)\end{aligned}$$

Here, the subscripts on the F/Q terms indicate the blocked boundary condition (BC), which is a virtual boundary for the stiffness (*F/Q*) type FRF; $\bar{Q}$ indicates

the displacements in the 6 dimensions for the 3 paths. For example, the blocked BC for $\mathrm{F}_{i;\,q}/Y_1$ in Equation (4) is $X_1 = Z_1 = \Psi_1 = \cdots = \Theta_3 = \Phi_3 = 0$, but only $Y_1 \neq 0$. If the stiffness type FRFs are available, the estimation process could be much simpler, since the matrix inversion will no longer be required. However, it is difficult to implement the true blocked BCs in experiments, though it is computationally possible [14]. Conversely, the free BCs, which are employed with the compliance (*Q/F*) type FRFs, are easy to implement. Thus Equation (2) is usually employed.

In Equation (4), each term $\left(\mathrm{F}_{i;\,q}/Q_n\right)Q_n$ may be considered as partial force or moment. The partial forces in terms of contributions from the 6 dimensional motions as $\sum_{n=1}^{3}\mathrm{F}_{3;\,q}/Q_n\big|_{\text{Blocked BC}}\,Q_n$ (Q = X, Y, Z, Ψ, Θ or Φ) are plotted in Figure 4.

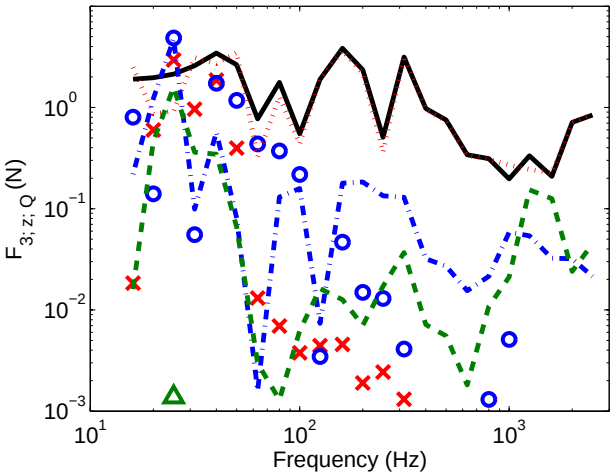

Figure 4. Partial force of $F_{3;z}$ magnitude spectra (on one third octave band basis). The 3-path sum as given by Equation (4); key: ——, $F_{3;z}$ (total); X, x-term; O, y-term; · · · · · ·, z-term; — · — · —, ψ-term; — — —, θ-term; △, φ-term.

It is observed that all of the 6-dimensional terms (except the φ-term) are observed over the low frequency region. Beyond that frequency, the partial force about the z-direction in the 3-path sum becomes most dominant, followed by the ψ- and θ-terms. It is because the original force is in the z-direction, and rotations about x and y axes contribute to the displacement z. Note that the z-term is one order of magnitude higher than the ψ- and θ-terms. Thus, the relative contributions of the ψ- and θ-terms are small. The φ-term is much smaller than other 5 dimensions, but it could include some errors inherent to the FEM code [12].

Finally, the sound pressure $p(\omega)$ at a receiver (microphone) location at any frequency is reconstructed as a vector sum of (complex-valued) partial sound pressures. This process attempts to relate structure-borne vibration paths to sound pressure (noise) at a point. In the experimental TPA method, acoustic FRFs p/F, accelerances a/F, and operational accelerations a are typically used for the all path locations. Note that the structural and acoustic FRFs should be measured without the source structure [1].

$$p(\omega) = \sum_{i=1}^{3} p_i(\omega) = \left[\frac{p}{\mathbf{F}}\right]\left(\left[\frac{\mathbf{a}}{\mathbf{F}}\right]^{-1}\mathbf{a}\right) \tag{5}$$

$$\text{where } p_i(\omega) = \sum_{i=1}^{3}\left[\frac{p}{\mathbf{F}_i}\right]\mathbf{F}_i \tag{6}$$

Here, $p/\mathbf{F}_i = \left(p/F_{i,x},\ p/F_{i,y},\ p/F_{i,z},\ p/N_{i,\psi},\ p/N_{i,\theta},\ p/N_{i,\varphi}\right)$ are acoustic FRFs. In the above expression, the apparent mass F/a has to be obtained by inverting the accelerance matrix $\left[\mathbf{a}/\mathbf{F}\right]^{-1}$. The partial sound pressure p_i corresponding to path *i* is compared each other. It should be noted that Equation (5) (with the exact forces) does not exactly reconstruct sound pressure, and the partial sound pressures inherently contain errors to some extent. One reason is that the sound radiated from the source structure is not included when the acoustic FRF is estimated.

ANALYSIS OF ERRORS ASSOCIATED WITH MISSING DIMENSIONS

ONE-DIMENSIONAL FORMULATIONS

Equation (2) exactly reconstructs the interfacial path forces. The inversion of the complete compliance matrix $\mathbf{H}$ of dimension *d* generally produces the exact dynamic stiffness matrix $\mathbf{D}$ of dimension *d*. Here, "complete" implies to completely determine the dynamics of the involved variables. However, many estimations utilize only limited dimensions, such as *d* = 1 and 3 at each point, rather than the general case of *d* = 6. Therefore, we analyze the errors associated with missing dimensions. First, consider the *d* = 1 case in the vertical z-direction; the interfacial path force estimated by indirect method (designated as the 1DOF (Z) formulation) for the 3-path system is:

$$\begin{pmatrix} F_{1;\,z} \\ F_{2;\,z} \\ F_{3;\,z} \end{pmatrix}_{1\text{DOF (Z)}} = \begin{pmatrix} \frac{Z_1}{F_{1;\,z}} & \frac{Z_1}{F_{2;\,z}} & \frac{Z_1}{F_{3;\,z}} \\ \frac{Z_2}{F_{1;\,z}} & \frac{Z_2}{F_{2;\,z}} & \frac{Z_2}{F_{3;\,z}} \\ \frac{Z_3}{F_{1;\,z}} & \frac{Z_3}{F_{2;\,z}} & \frac{Z_3}{F_{3;\,z}} \end{pmatrix}^{-1}_{\text{P-R}} \begin{pmatrix} Z_1 \\ Z_2 \\ Z_3 \end{pmatrix} \tag{7a}$$

$$F_{i;\,z}\big|_{1\text{DOF (Z)}} = \sum_{n=1}^{3}\frac{F_{i;\,z}}{Z_n}\bigg|_{1\text{DOF (Z)}} Z_n \tag{7b}$$

Compare the above 1DOF (Z) formulation with the exact 6DOF formulation given by Equation (2). Note that

$F_{i;z}/Z_n\big|_{1\mathrm{DOF}(Z)}$ is defined through the matrix inversion in Equation (7a), and it is not the exact dynamic stiffness, since a matrix with an incomplete dimension is inverted. Such a term may be called as "pseudo" dynamic stiffness. Since the exact dynamic stiffness estimation results in the exact indirect force estimation, the accuracy of the 1DOF (Z) formulation would depend on the accuracy of the dynamic stiffness estimated through the matrix inversion. Figure 5 shows the dynamic stiffness spectra estimated by the exact 6DOF and 1DOF (Z) formulations. Observe that the dynamic stiffness estimated in the 1DOF (Z) formulation converges well to the exact dynamic stiffness in the higher frequency region. Another point to observe is that the dynamic stiffness in the z-direction ($F_{3;z}/Z_3$) is much larger than the ones in the x- and y-directions, though the original compliances are of similar magnitudes (not shown). Therefore, the 1DOF (Z) formulation should work well under such conditions.

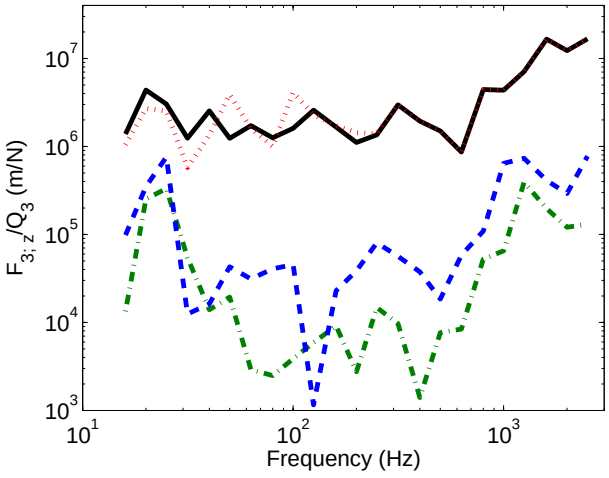

Figure 5. Dynamic stiffness (on one third octave band basis) with respect to $F_{3;z}$ for the path-receiver subsystem estimated by inverting the compliance matrix. Key: - · - · -, $F_{3;z}/X_3\big|_{6\mathrm{DOF}}$; - - - -, $F_{3;z}/Y_3\big|_{6\mathrm{DOF}}$; ——, $F_{3;z}/Z_3\big|_{6\mathrm{DOF}}$. ·····, $F_{3;z}/Z_3\big|_{1\mathrm{DOF}(z)}$.

Two types of error are, however, produced by the 1DOF (Z) formulation especially in the lower frequency region. First, error can be caused by a shift in the natural frequency bases. The operational responses Z_n and $F_{i;z}$ are measured in the entire S-P-R system in Equation (7), whereas FRFs $Z_n/F_{i;z}$ are measured in the P-R sub-system. Therefore, the Z_n (and $F_{i;z}$) terms and the $F_{i;z}/Z_n$ terms have different natural frequency bases. Thus the natural (resonance) frequency shift of $F_{i;z}/Z_n$ could cause fake resonances in $F_{i;z}$ estimation in Equation (7), though the shift is canceled out in the 6 dimensional formulation (Figure 3). Another cause of the errors is associated with matrix size reduction through the matrix inversion process. If very small numbers are present before the inversion, much larger force levels would be estimated through the matrix size reduction. Figure 6 compares force $F_{3;z}$ estimated by the 6DOF and 1DOF (Z) formulations on 1/3 octave band basis. The high peaks around 100 and 170 Hz in Figure 6 and peaks around 50 and 100 Hz in Figure 5 may be attributed to this problem. The 1DOF formulation could lead a large error especially in the low frequency region.

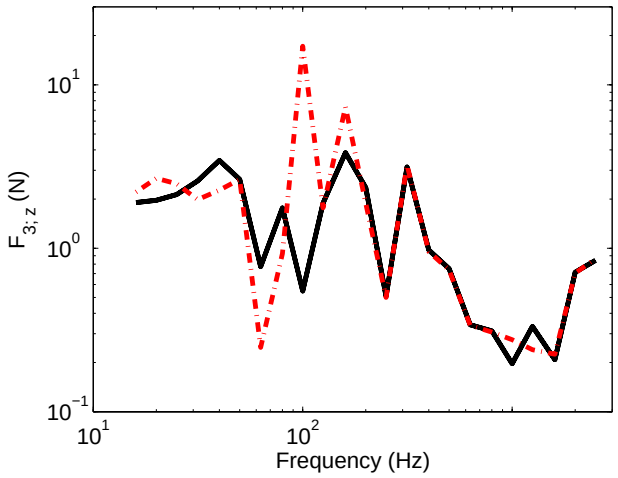

Figure 6. Interfacial path force magnitude spectra in the z-direction at the junction of source and path 3 (on one third octave band basis). Key: ——, direct and indirect 6DOF formulations; - · - · -, 1DOF (Z) formulation.

Based on the forces estimated by the indirect methods, sound pressure is reconstructed by Equation (5). Figure 7 compares the sound pressure directly estimated by BEM with the sound pressure indirectly estimated by the 6DOF and 1DOF (Z) formulations.

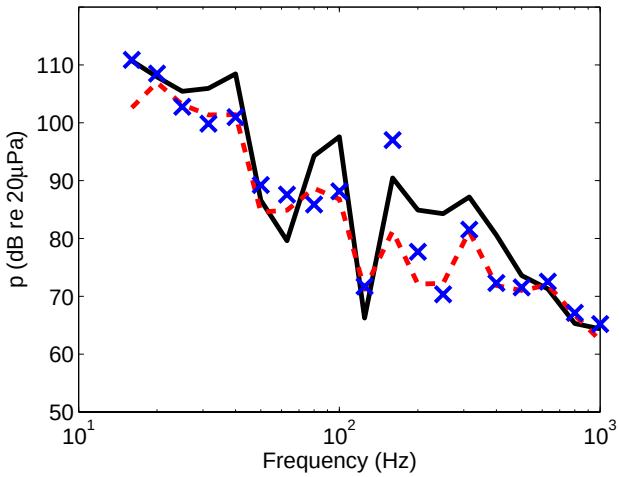

Figure 7. Sound pressure (total) magnitude on one third octave band basis. Key: ——, direct estimation; - - - -, 6DOF formulation; X, 1DOF (Z) formulation.

Observe that the use of the exact force in Equation (5) also yields errors to some extent in the indirect sound pressure estimation. Thus, at the frequency where the error is significant, caution must be exercised for the subsequent partial sound pressure used in TPA. Also, observe that the sound pressure estimated by the 1DOF (Z) formulation fluctuates around the 6DOF formulation result, and the accuracy of 1DOF (Z) formulation does not always follow that of the 6DOF formulation.

THREE-DIMENSIONAL FORMULATIONS

One may pose the next question as: Is there an effective formulation between *d* = 1 and *d* = 6? To answer this question, consider the indirect method in terms of the 3-translational dimensions (x, y and z), and estimate force in the z-direction of path *i*. This estimation may be called as the 3DOF (X, Y, Z) formulation.

$$F_{i;z}\Big|_{\substack{3\mathrm{DOF}\\(X,Y,Z)}} = \sum_{n=1}^{3}\left(\frac{F_{i;z}}{X_n}\Big|_{\substack{3\mathrm{DOF}\\(X,Y,Z)}} X_n + \frac{F_{i;z}}{Y_n}\Big|_{\substack{3\mathrm{DOF}\\(X,Y,Z)}} Y_n + \frac{F_{i;z}}{Z_n}\Big|_{\substack{3\mathrm{DOF}\\(X,Y,Z)}} Z_n \right) \tag{8}$$

Next, consider 3DOF (Z, Ψ, Θ) formulation, since the rotations about the x and y axes contribute to the translational motion in the z-direction.

$$F_{i;z}\Big|_{\substack{3\mathrm{DOF}\\(Z,\Psi,\Theta)}} = \sum_{n=1}^{3}\left(\frac{F_{i;z}}{Z_n}\Big|_{\substack{3\mathrm{DOF}\\(Z,\Psi,\Theta)}} Z_n + \frac{F_{i;z}}{\Psi_n}\Big|_{\substack{3\mathrm{DOF}\\(Z,\Psi,\Theta)}} \Psi_n + \frac{F_{i;z}}{\Theta_n}\Big|_{\substack{3\mathrm{DOF}\\(Z,\Psi,\Theta)}} \Theta_n \right) \tag{9}$$

Figure 8 compares path 3 force spectra that are produced by the 6DOF, 3DOF (X, Y, Z) and 3DOF (Z, Ψ, Θ) formulations. More errors are observed in the lower frequency region. Observe that the 3DOF (Z, Ψ, Θ) formulation does not always yield better estimation than the 3DOF (X, Y, Z) formulation. It is because the matrix inversion process could induce more errors in the 3DOF (Z, Ψ, Θ) formulation.

Furthermore, Figure 9 shows the three-dimensional force magnitude of path 3 ($|F_3| = \sqrt{F_{3;x}^2 + F_{3;y}^2 + F_{3;z}^2}$). Since the 1DOF formulation gives only 1-dimensional force, more errors occur over the entire frequency region by the 1DOF (Z) formulation, though $F_{3;z}$ is much greater than $F_{3;x}$ or $F_{3;y}$ in magnitude in most of frequencies (not shown). However, the 3DOF (X, Y, Z) formulation still agrees well with the exact 3-dimensional force magnitude as predicted by the 6DOF formulation. The error introduced by the 1DOF formulation is particularly noticeable at higher frequencies, when compared with Figure 6. This result indicates that although the 1DOF formulation could estimate force in the dominant direction, it may not be capable of predicting the force magnitude in the 3 dimensions.

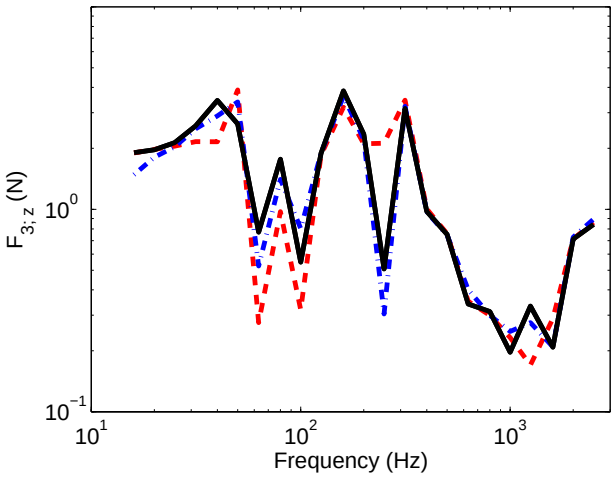

Figure 8. Interfacial path force magnitude spectra in the z-direction at the junction of source and path 3 (on one third octave band basis). Key: ———, direct and indirect 6DOF formulations; – – –, 3DOF (Z, Ψ, Θ) formulation; ·–·–·, 3DOF (X, Y, Z) formulation.

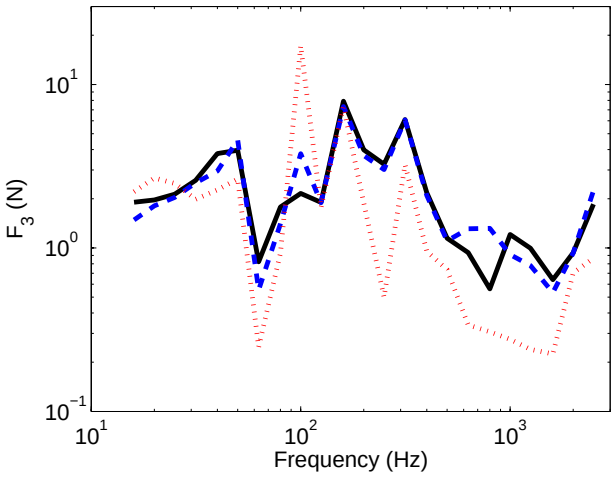

Figure 9. Interfacial path force magnitude spectra at the junction of source and path 3 (on one third octave band basis). Key: ———, direct and indirect 6DOF formulations; – – –, 3DOF (X, Y, Z) formulation; ▪ ▪ ▪ ▪, 1DOF (Z) formulation.

The sound pressure is next estimated by the 3DOF (X, Y, Z) and 3DOF (Z, Ψ, Θ) formulations based on Equation (5) where the sub-matrix and vector are used for the limited dimensional formulations. Figure 10 compares the estimated sound pressures with the estimations by the direct and 6DOF formulations. The 3DOF formulations yield somewhat better sound pressure estimations than the estimation by the 1DOF (Z) formulation shown in Figure 7, if they are compared with the estimation by the 6DOF formulation. However,

caution must be still exercised in the frequency bands where the error from the direct estimation is noticeable.

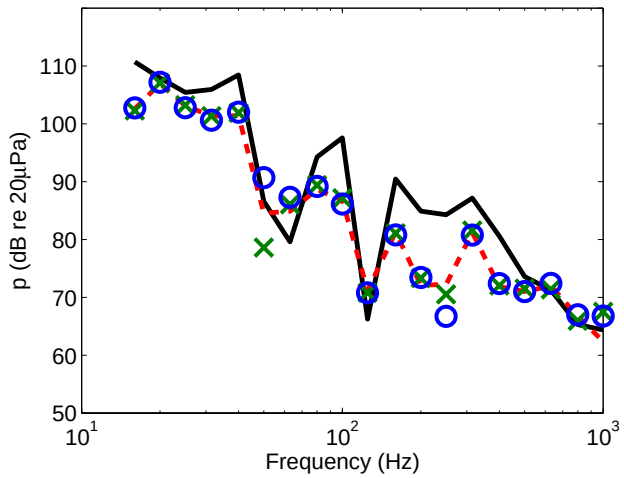

Figure 10. Sound pressure (total) magnitude on one third octave band basis. Key: ——, direct estimation; — — —, 6DOF formulation; **X**, 3DOF (X, Y, Z) formulation; **O**, 3DOF (Z, Ψ, Θ) formulation.

EFFECT OF MISSING DIMENSION ON PATH MEASURES AND RANK ORDERS

The partial sound pressure level is estimated by Equation (6), using the forces obtained by the four indirect methods; 6DOF, 3DOF (X, Y, Z), 3DOF (Z, Ψ, Θ) and 1DOF (Z) formulations. Table 1 shows the results, where the values relative to path 3 are given in deciBels (within the brackets). The path rank orders are found to qualitatively consistent among the indirect methods as a result of forces used for the determination of pressures. Path 3 is the most dominant, and path 1 is the least dominant in most frequency bands except around 1000 Hz. Recall that the reconstructed sound pressure itself is not exact, and thus even the 6DOF formulation would contain some errors.

Yet, another application of the interfacial force is the calculation of the dissipated powers. The time-averaged dissipated power in a system at any frequency may be formulated as follows [14].

$$\Pi(\omega)=\frac{1}{2}\mathrm{Re}\left[\mathbf{V}^{\mathrm{H}}\mathbf{F}\right]=\frac{1}{2}\mathrm{Re}\left[\mathbf{V}^{\mathrm{H}}\left(\tilde{\mathbf{K}}-\omega^2\mathbf{M}\right)\frac{\mathbf{V}}{j\omega}\right]=\frac{1}{2}\mathbf{V}^{\mathrm{H}}\mathbf{C}\mathbf{V}$$
$$=\frac{1}{2}\mathrm{Re}\left[\mathbf{V}_{\mathrm{Dr}}^{\mathrm{H}}\mathbf{F}_{\mathrm{Dr}}\right]\geq 0 \qquad (10)$$

Not only for a point but also for the system or a subset thereof are considered in Equation (10), and equations of motion of the system is substituted where **M, K** and **C** are the inertia, stiffness and viscous damping matrices of the system, respectively, and $\tilde{\mathbf{K}}=\mathbf{K}+j\omega\mathbf{C}$. The complex velocity amplitude vector is $\mathbf{V}=j\omega\mathbf{Q}$. The superscript H indicates conjugate transpose. Note that dissipated power can be estimated only from the driving point velocity and force. The dissipated power in path *i* (sub-system) is

$$\Pi_i=\frac{1}{2}\mathrm{Re}\left[\mathbf{V}_i^{\mathrm{H}}\mathbf{F}_i\right]-\frac{1}{2}\mathrm{Re}\left[\mathbf{V}_{i\mathrm{R}}^{\mathrm{H}}\mathbf{F}_{i\mathrm{R}}\right] \qquad (11)$$

where subscript *i*R indicates the P-R junctions. The total dissipated power in the paths is $\Pi_{\mathrm{P}}=\sum_{i=1}^{3}\Pi_i$, and dissipated power ratio of path *i* is Π_i/Π_{P} (*i* = 1, 2, 3). Figure 11 shows dissipated power ratio of path *i* to the total for paths (Π_i/Π_{P}) with 6DOF and 1DOF (Z) formulations.

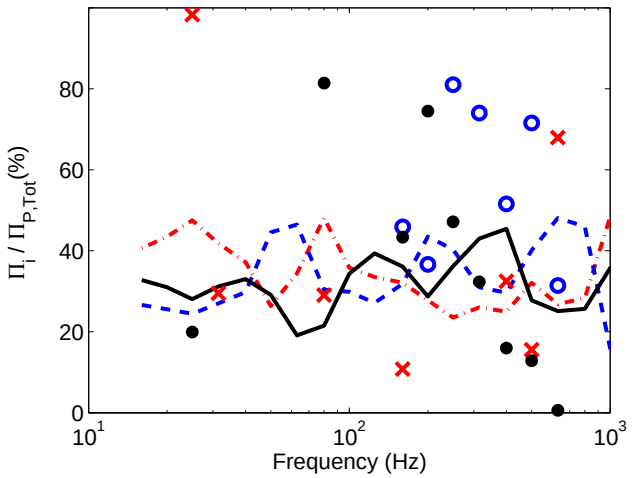

Figure 11. Dissipated power ratio of each path to the total of paths with *d* DOF formulation (on one third octave band basis). Key: ▪ — ▪ — ▪, path 1 (*d* = 6); — — —, path 2 (*d* = 6); ——, path 3 (*d* = 6); **X**, path 1 (*d* = 1; Z); **O**, path 2 (*d* = 1; Z); ●, path 3 (*d* = 1; Z). Only values between 0 and 100 % are shown for 1DOF formulation.

Note that power (ratio) estimated by formulation with *d* = 1 takes both positive and negative values, whose interpretation may be troublesome. Further, the ratio (for *d* = 1) may indicate a significantly large value. In the above example in Figure 11, at 50 Hz, power ratio estimated with *d* = 1 for path 3 is 1061%, and – 547% for path 2 (not shown). Thus a caution must be exercised in typical experimental estimations with *d* = 1. Meanwhile the power with 6DOF formulation is always positive, and thus power ratios show a clear path rank order in terms of power dissipation.

CONCLUSION

First, this paper has developed the indirect, yet exact, interfacial path force (and moment) estimation formulations, based on the 6-dimensional motions at each point. We have especially shown that forces can be exactly determined with only the driving point responses and FRFs. Since only the dynamic compliance (*X*/*F*) type translational FRFs are usually employed in experimental studies, our 6-dimensional formulation could be used to assess the errors that would be committed by formulations with *d* < 6.

The proposed formulations have been computationally illustrated using the system of Figure 1 with three parallel vibration transmission paths. We started with the standard 1DOF (Z) formulation, and then examined two intermediate, 3DOF (X, Y, Z) and 3DOF (Z, Ψ, Θ) formulations in terms of path force and sound pressure. Although the rotations about x and y axes contribute to the displacement in the z-direction, it seems that the matrix inversion process disturbs the order of dominance to some extent. Thus, the 3DOF (Z, Ψ, Θ) formulation might not always yield a better estimation than one or other three DOF formulations. We also examined the indirect methods for the power flow estimation. Our results indicate that limited formulation could yield negative power, though 6DOF formulation always yields positive power as defined.

The path rank order is somewhat consistent for our example structure, but it could be frequency-dependent in practical problems. Attempts should be made to further improve the indirect method for (partial) sound pressures.

ACKNOWLEDGMENTS

The Center for Automotive Research Industrial Consortium at The Ohio State University is gratefully acknowledged for supporting this research.

REFERENCES

1. LMS International, Application Notes. Transfer Path Analysis: The Qualification and Quantification of Vibro-acoustic Transfer Paths. http://www.lmsintl.com/
2. A. Inoue, S. Kim and R. Singh, Comparative Evaluation of Structure-borne Noise Transfer Paths in a Laboratory Experiment, Noise Control Engineering Journal, Vol. 54(6), pp 382-395, 2006.
3. J. Plunt, Examples of Using Transfer Path Analysis Together with CAE-models to Diagnose and Find Solutions for NVH Problems Late in the Vehicle Development Process, SAE Paper 2005-01-2508.
4. M.A. Gehringer, Application of Experimental Transfer Path Analysis and Hybrid FRF-based Substructuring Model to SUV Axle Noise, SAE Paper 2005-01-1833.
5. A.N. Thite and D.J. Thompson, The Quantification of Structure-borne Transmission Paths by Inverse Methods. Part 1: Improved Singular Value Rejection Methods, Journal of Sound and Vibration, Vol. 264(2), pp 411-431, 2003.
6. A.N. Thite and D.J. Thompson, Selection of Response Measurement Locations to Improve Inverse Force Determination, Applied Acoustics, Vol. 67(8), pp 797-818, 2006.
7. Q. Leclere, C. Pezerat, B. Laulagnet and L. Polac, Indirect Measurement of Main Bearing Loads in an Operating Diesel Engine, Journal of Sound and Vibration, Vol. 286(1-2), pp 341-361, 2005.
8. R. Singh and S. Kim, Examination of Multi-dimensional Vibration Isolation Measures and Their Correlation to Sound Radiation over a Broad Frequency Range, Journal of Sound and Vibration, Vol. 262(3), pp 419-455, 2003.
9. M.A. Sanderson and C.R. Fredo, Direct Measurement of Moment Mobility, Part 2: An Experimental Study, Journal of Sound and Vibration, Vol. 179(4), pp 685-696, 1995.
10. L. Ivarsson and M.A. Sanderson, MIMO Technique for Simultaneous Measurement of Translational and Rotational Mobilities, Applied Acoustics, Vol. 61(3), pp 345-370, 2000.
11. P. Gardonio and S.J. Elliott, Passive and Active Isolation of Structural Vibration Transmission between Two Plates Connected by a Set of Mounts, Journal of Sound and Vibration, Vol. 237(3), pp 483-511, 2000.
12. Ansys Inc. ANSYS User's Manual Online, version 10, 2006.
13. LMS International N. V. Release Notes and Getting Started Manual. LMS Sysnoise rev 5.6, 2003.
14. A. Inoue, S. Kim and R. Singh, Effect of Rotational Motions on the Estimation of Interfacial Path Forces and Structure-borne Noise Path Rank Orders, *Submitted to the Applied Acoustics*, July 2006.

CONTACT

Professor Rajendra Singh
Acoustics and Dynamics Laboratory
Center for Automotive Research
The Ohio State University
Email: singh.3@osu.edu
Phone: 614-292-9044
Website: www.AutoNVH.org

Table 1. Partial sound pressure magnitudes as estimated by Equation (6), where path forces are estimated by the following four indirect methods: 6DOF, 1DOF (Z), 3DOF (X, Y, Z), and 3DOF (Z, Ψ, Θ). The number within bracket is the relative value (in dB) compared with path 3 which is assigned a value of 0 dB.

Octave Band Center Frequency (Hz)	Partial Sound Pressure (dB re 20 μPa) Based on Formulation											
	6DOF			1DOF (Z)			3DOF (X,Y,Z)			3DOF (Z,Ψ,Θ)		
	P1	P2	P3	P1	P2	P3	P1	P2	P3	P1	P2	P3
16	88 [-29]	112 [-5]	117 [0]	67 [-53]	115 [-5]	120 [0]	101 [-12]	106 [-7]	113 [0]	91 [-27]	112 [-6]	118 [0]
31.5	77 [-32]	102 [-7]	109 [0]	89 [-18]	97 [-10]	107 [0]	76 [-32]	101 [-7]	108 [0]	65 [-42]	98 [-9]	107 [0]
63	75 [-18]	89 [-4]	93 [0]	71 [-19]	85 [-5]	90 [0]	78 [-16]	91 [-3]	94 [0]	74 [-19]	92 [-1]	93 [0]
125	70 [-11]	79 [-2]	81 [0]	79 [-7]	75 [-11]	86 [0]	72 [-9]	79 [-2]	81 [0]	74 [-7]	79 [-2]	81 [0]
250	65 [-13]	78 [0]	78 [0]	62 [-16]	77 [-1]	78 [0]	64 [-13]	78 [0]	78 [0]	67 [-13]	79 [1]	80 [0]
500	63 [+1]	62 [0]	62 [0]	63 [-1]	63 [+1]	62 [0]	63 [+1]	63 [+1]	62 [0]	64 [+2]	62 [0]	62 [0]
1000	56 [+1]	59 [+4]	55 [0]	57 [-5]	58 [+6]	52 [0]	57 [+6]	58 [+7]	51 [0]	57 [+10]	58 [+11]	47 [0]
2000	55 [-10]	61 [-4]	65 [0]	55 [-11]	58 [-8]	66 [0]	53 [-13]	57 [-9]	66 [0]	54 [-10]	60 [-4]	64 [0]